J. Fluid Mech. (2010), *vol.* 650, *pp.* 363–389.
doi:10.1017/S002211200999348X

Interfacial instability due to evaporation and convection: linear and nonlinear analyses

W. GUO AND R. NARAYANAN†

Department of Chemical Engineering, University of Florida, Gainesville, FL 32611, USA

(Received 3 September 2008; revised 14 November 2009; accepted 16 November 2009; first published online 15 March 2010)

Interfacial instability arising from evaporation of a single component liquid is investigated using linear and weakly nonlinear analysis. Evaporative convection is studied taking into account the fluid dynamics of both liquid and vapour phases as well as lateral rigid sidewalls. Both open and closed systems are addressed. The nature of the bifurcation and the change in heat flux in the nonlinear regime are determined. It is shown that depending upon the aspect ratio of the geometry, either supercritical or subcritical branching behaviour is possible.

1. Introduction

Evaporation from a liquid in contact with its vapour can lead to an instability that is manifested by the onset of surface undulations and non-uniform velocity fields. This instability may occur even in the absence of gravity or surface tension gradient effects. Consider a typical evaporation process as depicted in figure 1. In such a process, the input variables are the fluid depths and the temperature difference across the layers. If the upper and lower boundaries are impermeable, we have a closed system and the net average evaporative flux must be zero; the pressure at the top plate is an output variable as are the velocity and temperature profiles and surface shape. However, if the upper and lower walls are permeable porous plates, we have an open system and the pressure external to the top plate must also be assigned. In order to maintain a steady state, the pressure external to the bottom plate depends on this top pressure via a hydrostatic balance and the pressure drop across the porous walls. The total evaporative flux in such an open system becomes yet another output variable. Regardless of whether we have an open or closed system, the mechanism for the instability is the same. It bears some similarity to that of the morphological instability seen in the solidification of a pure substance. To see why, let us consider an evaporating layer with a heated liquid as in figure 1. A mechanical perturbation at the deflecting interface is reinforced as liquid thermal gradients at a trough become stronger, while vapour thermal gradients become weaker. The evaporation rate then increases as it depends on the difference in heat flux at the interface. As this difference becomes greater, a trough becomes deeper. The reverse situation occurs at a crest, i.e. crests become steeper. Surface tension comes in to stabilize the disturbance as do viscous and thermal relaxations, helping in the selection of a wavelength. This physical argument for the instability does not require the interface to be deflectable. In fact, when the interface is taken to be flat, the instability establishes because a temperature perturbation at the interface generates a local cold spot (for example),

† Email address for correspondence: ranga@ufl.edu

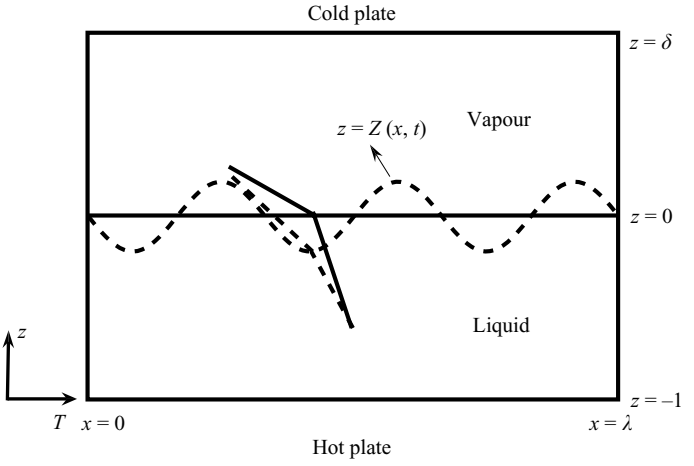

FIGURE 1. Schematic of two-phase evaporation depicting the instability. The dotted lines refer to the perturbed interface and the perturbed local gradients while the solid lines refer to the unperturbed or base interface and the base local gradients.

which drives more heat to it, causes evaporation and cools it even further. This evaporative flow is weak in the liquid and strong in the vapour on account of the disparate densities of the two phases. The process saturates to a steady state with a definite wavelength on account of viscous and thermal diffusion. If the vapour is taken to be passive, there are no transverse flows in the vapour phase and so hot flows from high pressure evaporating regions cannot flow to cooler lower pressure regions and help reign in the instability.

To put the present work in the context of earlier studies, it is helpful to place the past research into broad categories where (*a*) the upper phase is taken to be fluid dynamically either passive or active, (*b*) the entire system is either closed or open, (*c*) the control variable to initiate the instability is either an assigned temperature drop across the system or the pressure at an upper location away from the interface, (*d*) the upper phase is either pure or contains an inert gas, and (*e*) the thermodynamic equilibrium is assumed at the interface versus assuming a non-equilibrium relation involving mass exchange.

The early work of Burelbach, Bankoff & Davis (1988) and recent works by Margerit, Dondlinger & Dauby (2005, 2006) and Oron (1999) dealt with fluid mechanically passive vapour layers; both sets of studies included thermocapillary convection and both addressed nonlinear aspects of the instability in open systems. Burelbach *et al.* (1988) derived long wavelength approximations in which the temperature drop across a thin layer was taken to be the control variable. They then considered conditions for dry-out using a non-equilibrium relation for interfacial mass exchange. Margerit *et al.*'s work predicted the nonlinear evaporation rates in an open system with an inert gas, assuming thermodynamic and thermal equilibrium at the interface. The control of the instability in their case was obtained by adjusting the upper gas pressure. Their main interest was in predicting the stability of various planforms in infinitely wide layers. Contrasting these works are those that include fluid mechanics in the upper vapour phase. Among these are the works of Huang & Joseph (1992), Ozen & Narayanan (2004*a*,*b*), Haut & Colinet (2005) and McFadden *et al.* (2007). Using

linearized stability methods, Huang & Joseph (1992) analysed an infinitely wide bilayer heated from above and showed that the instability must begin as oscillatory motion, i.e. via Hopf bifurcations. A major result of their work is that for low evaporation rates, there is little difference between assuming thermal equilibrium along with thermodynamic equilibrium versus assuming a temperature jump and thermodynamic equilibrium between the pressure and the temperature at the interface in each phase. Ozen & Narayanan showed for unbounded regions that when the liquid is heated the instability is delayed when flow in the vapour becomes strong. Their reasoning was based on the large flows in the vapour carrying heat from high-pressure hot regions to low-pressure cold regions. The effect of vapour height on fluid motion in the vapour phase accounting for inert gas motion was the essence of the work of Haut & Colinet (2005). Their analysis showed that the absence of inert gases reduces the effect of Marangoni motion substantially and thin vapour heights reduce vapour flow as well. Recent theoretical work involving fluid flow in the vapour is due to McFadden *et. al.*, who showed that the entropy difference between the phases near the thermodynamic critical state has an immense impact on the instability. There is limited experimental work on evaporative instability to confirm any of the above theories. A recent report by Zhang (2006) suggests that buoyancy convection plays an important role in all but very thin layers. His experiments were done in the presence of inert gases in the vapour phase.

In contrast with earlier work, our interest is in understanding the physics of the instability in open and closed configurations where lateral walls are included and where the base state is strictly a steady state. As the vapour flow tends to dampen the instability, the role of sidewall proximity is dual. It can dampen the liquid flow and enhance stability or dampen vapour flow and enhance instability. Understanding this dual role is one aspect of this work. Another aspect is to determine the nature of the bifurcation behaviour as the sidewall proximity changes. This is important as working in regimes of supercritical bifurcation is experimentally desirable to make a connection with predictions. Finally, buoyancy-driven flows combined with evaporation act differently than pure evaporation in closed versus open systems. This too is of interest on account of microgravity applications and is also a subject of our discussion. Our work will reveal the non-monotonic nature of the critical temperature difference with aspect ratio when buoyancy is taken into account but not otherwise.

2. Formulation of the problem

To analyse a concrete problem, we consider a two-dimensional rectangular container with a liquid such as water or alcohol underlying its own vapour. Both fluid phases are taken to be of finite extent. The top and bottom walls are assumed to be perfectly conducting, with the bottom wall temperature higher than the top. The vertical sidewalls are taken to be perfectly insulating and the free surface is allowed to deflect. Imagine as a first case that the top vapour phase is devoid of all inert gases and that the system is closed, i.e. the top and bottom walls are impermeable. This means that the net evaporative flux must be zero as long as the vapour phase is assumed to be incompressible, a very reasonable assumption in most instances. Under such circumstances, phase change is allowed only through perturbations at the interface; in other words, the total evaporative flux is zero, whereas the local flux need not be so. A second case considered below allows the upper and lower walls to be permeable. The pressures at the exterior of the upper and lower walls are additional input variables.

As in the first case, the temperature difference between the plates is controlled until the instability sets in. A possible variant on the second case is to make the wall temperatures equal to one another and to control the upper plate pressure until the instability commences. However, this variant on the second case is not considered as it does not add anything substantially new. Each of the two cases under consideration is interesting in its own right, yielding qualitatively different results. We now move on to the case of impermeable walls and zero total evaporative flux, first giving the nonlinear equations that govern the phenomena, then analysing these equations by linearized and weakly nonlinear methods.

3. The nonlinear equations

The modelling equations are nonlinear on several counts. The principal reason is that the local evaporation rate must depend on the local temperature gradients at the interface, thus making the velocity field a functional of the temperature field. In the absence of buoyancy or surface tension gradients, the dependence of the velocity perturbations on the temperature field arises from the coupling between the latter and the pressure field at the interface. This makes the convective heat transfer a quadratic functional of temperature. In addition to this nonlinearity, the curvature of the interface is a nonlinear functional of its position. These nonlinearities are behind the instability phenomena associated with evaporation.

The nonlinear equations are put into scaled form using d, the liquid depth, for the length scale, κ/d for the velocity scale, d^2/κ for the time scale and $\mu\kappa/d^2$ for the pressure scale while the temperature is measured with respect to the cold plate temperature T_{cold} and scaled by the temperature drop across the system ($T_{hot} - T_{cold}$). Here, the symbols ν, κ and μ are the kinematic viscosity, the thermal diffusivity and the dynamic viscosity, respectively.

We begin by giving the scaled momentum equations in each phase, which are

$$\frac{1}{Pr}\left(\frac{\partial \boldsymbol{v}}{\partial t} + \boldsymbol{v}\cdot\nabla\boldsymbol{v}\right) = -\nabla\Pi + \nabla^2\boldsymbol{v} + RaT$$

and

$$\frac{\nu}{\nu^*}\frac{1}{Pr}\left(\frac{\partial \boldsymbol{v}^*}{\partial t} + \boldsymbol{v}^*\cdot\nabla\boldsymbol{v}^*\right) = -\frac{\mu}{\mu^*}\nabla\Pi^* + \nabla^2\boldsymbol{v}^* + \frac{\alpha^*}{\alpha}\frac{\nu}{\nu^*}RaT^*.$$

The scaled energy equations in each phase are

$$\frac{\partial T}{\partial t} + \boldsymbol{v}\cdot\nabla T = \nabla^2 T$$

and

$$\frac{\partial T^*}{\partial t} + \boldsymbol{v}^*\cdot\nabla T^* = \frac{\kappa^*}{\kappa}\nabla^2 T^*.$$

The continuity equations in each phase are

$$\nabla\cdot\boldsymbol{v} = 0$$

and

$$\nabla\cdot\boldsymbol{v}^* = 0.$$

In the equations above, the asterisk denotes the vapour phase, $\boldsymbol{v}$ and T are the scaled velocity and temperature fields, while Π conveniently expresses the modified

scaled pressure field. It differs from the usual scaled pressure field, P, by the scaled static liquid head, i.e.

$$\nabla \Pi = \nabla P + \frac{\rho g d^3}{\mu \kappa} \boldsymbol{k},$$

where $\boldsymbol{k}$ is the unit base vector in the positive z direction. The dimensionless groups Pr and Ra are the liquid Prandtl and Rayleigh numbers, where Ra is defined as $Ra = (\alpha g (T_{hot} - T_{cold}) d^3)/\nu\kappa$ and where the thermal expansion coefficient is denoted by α. Absent from each of the energy equations is a term arising from viscous dissipation. Using the scale factors above, we see easily that such terms are of $O(10^{-15})$ and may therefore be discarded in comparison with the diffusive terms.

At the top and bottom walls, located at $z = \delta$ and $z = -1$, the temperatures are kept constant while no-slip and no mass transfer conditions apply. The sidewalls, located at $x = 0$ and λ, are assumed to be perfectly insulating and impermeable to mass transfer. Here λ is the scaled width, i.e. the aspect ratio, and δ is the scaled upper-phase depth. For the case of rigid vertical walls, we assume that no-slip holds. Denoting the interface position by $Z(x, t)$, we assume for the case of rigid walls that $Z = 0$ at $x = 0, \lambda$, i.e. a fixed contact condition holds. This is a physically realizable condition for liquid–vapour interfacial instability experiments as shown by Ozen *et al.* (2005). It corresponds to experiments with a pinning edge at the sidewalls. Such edges disallow a meniscus to be formed. For the case when the walls are taken to be slippery, a traction-free surface is assumed in addition to $\partial Z/\partial x = 0$; this is a free contact condition and is of theoretical interest, rather than of practical value.

Observe that this problem is an initial value problem, and in the cases under consideration it can be easily shown from divergence-free velocity fields and the interfacial mass balance that the volumes of the fluid regions must be constants in time. We now turn to the boundary conditions obtained from the jump phase balances (cf. Slattery 1990) under the restriction that the interface is singular, possessing only surface tension but not any surface viscosity. This is reasonable for pure substances (cf. Edwards, Brenner & Wasan 1991).

The mass balance at the interface, $z = Z(x, t)$, is

$$(\boldsymbol{v} - \boldsymbol{u}) \cdot \boldsymbol{n} = \frac{\rho^*}{\rho} (\boldsymbol{v}^* - \boldsymbol{u}) \cdot \boldsymbol{n}. \tag{3.1}$$

Here ρ and ρ^* are the liquid density and vapour density, respectively, and the unit outward normal, $\boldsymbol{n}$, is given by

$$\boldsymbol{n} = \frac{-\partial Z/\partial x \boldsymbol{i} + \boldsymbol{k}}{\left[1 + (\partial Z/\partial x)^2\right]^{1/2}},$$

while the interfacial speed, $\boldsymbol{u} \cdot \boldsymbol{n}$, is given by

$$\boldsymbol{u} \cdot \boldsymbol{n} = \frac{\partial Z/\partial t}{\left[1 + (\partial Z/\partial x)^2\right]^{1/2}}.$$

The continuity of tangential component of velocity at the interface yields $\boldsymbol{v} \cdot \boldsymbol{t} = \boldsymbol{v}^* \cdot \boldsymbol{t}$. Here $\boldsymbol{t}$ represents the unit tangent vector, which is given by

$$\boldsymbol{t} = \frac{\boldsymbol{i} + (\partial Z/\partial x)\boldsymbol{k}}{\left[1 + (\partial Z/\partial x)^2\right]^{1/2}}.$$

The interfacial force balance equation in scaled form becomes

$$Ca\left[\frac{1}{Pr}\boldsymbol{v}(\boldsymbol{v}-\boldsymbol{u})-\frac{\rho^*}{\rho}\frac{1}{Pr}\boldsymbol{v}^*(\boldsymbol{v}^*-\boldsymbol{u})\right]\cdot\boldsymbol{n}-Ca\,Ma\nabla_S T\boldsymbol{t}+2H\boldsymbol{n}=Ca(\boldsymbol{T}-\boldsymbol{T}^*)\cdot\boldsymbol{n},\quad(3.2)$$

where $\boldsymbol{T}=-P\boldsymbol{I}+\boldsymbol{S}$ is the total stress with P being the scaled pressure and $\boldsymbol{S}$ is the extra viscous stress tensor. In addition, $Ca=\mu\kappa/\gamma d$ is the Capillary number and γ is the interfacial tension, while the Marangoni number, Ma, is defined as $Ma=(\gamma_T(T_{hot}-T_{cold})d)/\mu\kappa$, with γ_T being the negative of the surface tension gradient with respect to temperature, and $2H=\partial^2 Z/\partial x^2/[1+(\partial Z/\partial x)^2]^{3/2}$ is twice the surface mean curvature.

The energy balance at the interface is

$$\left\{-1+K_{PC}\left[\frac{1}{2}(\boldsymbol{v}-\boldsymbol{u})^2-\frac{1}{2}(\boldsymbol{v}^*-\boldsymbol{u})^2\right]\right\}(\boldsymbol{v}-\boldsymbol{u})\cdot\boldsymbol{n}$$
$$-E(\nabla T\cdot\boldsymbol{n}-\frac{k^*}{k}\nabla T^*\cdot\boldsymbol{n})-V_{PC}\left[\boldsymbol{S}\cdot(\boldsymbol{v}-\boldsymbol{u})-\frac{\mu^*}{\mu}\boldsymbol{S}^*\cdot(\boldsymbol{v}^*-\boldsymbol{u})\right]\cdot\boldsymbol{n}=0,\quad(3.3)$$

where $K_{PC}=\kappa^2/\pounds d^2$, $E=k(T_{hot}-T_{cold})/\rho\pounds\kappa$, $V_{PC}=\nu\kappa/\pounds d^2$, k is the liquid thermal conductivity and $\pounds$ is the latent heat per unit mass. Henceforth, E is termed the evaporation number.

In the closed container case the base evaporation rate is zero, and in the open container case the pressure is adjusted suitably such that the evaporation rate is zero because the qualitative nature of the instability does not depend on this assumption. In addition, the local evaporation is obtained from linearized stability and consequently assumed to be very small. Now, Ward & Stanga (2001) and Shankar & Deshpande (1990) have shown that the temperature jump across the interface is very small if the evaporation rate is also small. It is therefore valid to assume thermal equilibrium at the interface, i.e. $T=T^*$. In addition, we assume that local thermodynamic equilibrium at the interface holds via the familiar Clausius–Clapeyron equation, viz.

$$\Pi_{KE}(P^*-P^*_{base})=\ln\left(\frac{T^*}{T^*_{base}}\right),\quad(3.4)$$

where $\Pi_{KE}=(\rho/\rho^*)(\nu\kappa/\pounds d^2)$, P^*_{base} and T^*_{base} are the scaled interfacial pressure and temperature of the vapour in a reference state, i.e. P^*_{base} is the vapour pressure corresponding to T^*_{base}. A non-equilibrium relation (cf. Schrage 1953) would be appropriate for the case in which the scaled base evaporation rate is of $O(1)$ or greater.

In writing the Clausius–Clapeyron equation, the surface curvature's correction on the vapour pressure is ignored as the ratio of the vapour to liquid density is of $O(10^{-3})$ and is therefore very small. Unlike solidification where surface curvature acts to reduce the melt point via the Gibbs–Thomson effect and selects the wavelength of the instability, the corresponding change in typical liquid–vapour phase-change problems, called the Kelvin correction, is insignificant and plays little role in the selection of the wavelength, this being achieved by the surface tension that acts on the pressure difference at the interface. As observed by McFadden *et al.* (2007), this would not be the case when the fluids are near their thermodynamic critical state as the density difference between the vapour and the liquid is not large and the Kelvin correction attains importance. We now turn to the linear stability analysis for the first case, the closed container problem.

4. Linear stability analysis for the closed container case

4.1. *The base state solution and the linearized equations*

To study interfacial instability, we apply arbitrary infinitesimal disturbances to the domain state variables and linearize the domain and boundary equations about the base state, which in the closed container case corresponds to no flow in each phase. The base state temperature profiles, indicated by the subscript zero, become

$$T_0 = -\frac{k^*}{k\delta + k^*} z + \frac{k\delta}{k\delta + k^*}$$

and

$$T_0^* = -\frac{k}{k\delta + k^*} z + \frac{k\delta}{k\delta + k^*},$$

where $\delta = d^*/d$ is the ratio of vapour-to-liquid fluid depths.

Denoting the disturbance or deviation variables by the subscript 1 and assuming that they grow or die as $e^{\sigma t}$, where σ is an inverse growth or decay constant, we proceed to obtain the linearized perturbation equations in both phases. For the lower layer, the equations of motion become

$$\frac{\sigma}{Pr} v_{x1} = -\frac{\partial P_1}{\partial x} + \nabla^2 v_{x1}$$

and

$$\frac{\sigma}{Pr} v_{z1} = -\frac{\partial P_1}{\partial z} + \nabla^2 v_{z1} + Ra T_1.$$

The continuity equation is

$$\frac{\partial v_{x1}}{\partial x} + \frac{\partial v_{z1}}{\partial z} = 0$$

and the energy equation becomes

$$\sigma T_1 = \nabla^2 T_1 - \frac{\mathrm{d}T_0}{\mathrm{d}z} v_{z1}.$$

For the upper layer, we have likewise

$$\frac{\sigma}{Pr}\frac{\nu}{\nu^*} v_{x1}^* = -\frac{\mu}{\mu^*}\frac{\partial P_1^*}{\partial x} + \nabla^2 v_{x1}^*,$$

$$\frac{\sigma}{Pr}\frac{\nu}{\nu^*} v_{z1}^* = -\frac{\mu}{\mu^*}\frac{\partial P_1^*}{\partial z} + \nabla^2 v_{z1}^* + \frac{\alpha^*}{\alpha}\frac{\nu}{\nu^*} Ra T_1^*,$$

$$\frac{\partial v_{x1}^*}{\partial x} + \frac{\partial v_{z1}^*}{\partial z} = 0$$

and

$$\sigma \frac{\kappa}{\kappa^*} T_1^* = \nabla^2 T_1^* - \frac{\kappa}{\kappa^*}\frac{\mathrm{d}T_0^*}{\mathrm{d}z} v_{z1}^*.$$

At the interface, the linearized equation for the mass balance is

$$v_{z1} - \frac{\rho^*}{\rho} v_{z1}^* = \left(1 - \frac{\rho^*}{\rho}\right) \sigma Z_1. \tag{4.1}$$

Here, Z_1 is the perturbed interface position. It is the lowest order mapping of the deflected surface to the reference flat surface. The linearized equation for the no-slip

boundary condition at the interface is

$$v_{x1} = v_{x1}^*. \tag{4.2}$$

To these we add the linearized equations for normal and tangential stress, which are

$$Ca(P_1 - P_1^*) - 2Ca\left(\frac{\partial v_{z1}}{\partial z} - \frac{\mu^*}{\mu}\frac{\partial v_{z1}^*}{\partial z}\right) - BoZ_1 + \frac{\partial^2 Z_1}{\partial x^2} = 0, \tag{4.3}$$

where $Bo = ((\rho - \rho^*)gd^2)/\gamma$ is the Bond number and

$$\frac{\mu^*}{\mu}\left(\frac{\partial v_{x1}^*}{\partial z} + \frac{\partial v_{z1}^*}{\partial x}\right) - \left(\frac{\partial v_{x1}}{\partial z} + \frac{\partial v_{z1}}{\partial x}\right) - Ma\left(\frac{\partial T_1}{\partial x} + \frac{\mathrm{d}T_0}{\mathrm{d}z}\frac{\partial Z_1}{\partial x}\right) = 0. \tag{4.4}$$

We observe that the Bond number makes its appearance for the first time in (4.3). It arose when the perturbation of the pressure field P about the reference state is corrected by the mapping Z_1 times the difference of the base pressure gradients (Chandrasekhar 1961; Johns & Narayanan 2002). It would have arisen earlier in the nonlinear equation for the interfacial force balance, (3.2), had we chosen to express all of our formulas in terms of the modified pressure, Π, instead of the scalar pressure, P. As noted earlier, the difference between these two variables is the scaled static liquid head.

The interfacial energy balance and thermal equilibrium lead to

$$v_{z1} - E\left(\frac{k^*}{k}\frac{\partial T_1^*}{\partial z} - \frac{\partial T_1}{\partial z}\right) = \sigma Z_1 \tag{4.5}$$

and

$$T_1 + \frac{\mathrm{d}T_0}{\mathrm{d}z}Z_1 = T_1^* + \frac{\mathrm{d}T_0^*}{\mathrm{d}z}Z_1. \tag{4.6}$$

We now add the linearized Clausius–Clapeyron equation, viz.

$$\Pi_{KE}P_1^* - \Pi_{PE}Z_1 = \frac{T_1^* + (\mathrm{d}T_0^*/\mathrm{d}z)Z_1}{T_0^*}, \tag{4.7}$$

where $\Pi_{PE} = (gd)/\mathcal{L}$.

The remaining boundary conditions that must be linearized are those at the top, bottom and sidewalls. At the top wall, the perturbed velocity and temperature are zero. Hence,

$$v_{x1}^* = v_{z1}^* = T_1^* = 0 \quad \text{at } z = \delta$$

and so too at the bottom wall, where

$$v_{x1} = v_{z1} = T_1 = 0 \quad \text{at } z = -1$$

must hold.

At the sidewalls, the conditions for the upper fluid reflect no flow, no-slip and no heat transport, i.e.

$$v_{x1}^* = v_{z1}^* = \frac{\partial T_1^*}{\partial x} = 0 \quad \text{at } x = 0, \lambda.$$

Likewise, at the sidewalls, the conditions for the lower fluid are

$$v_{x1} = v_{z1} = \frac{\partial T_1}{\partial x} = 0 \quad \text{at } x = 0, \lambda.$$

$\rho = 960$ kg m^{-3}	$\rho^* = 0.6$ kg m^{-3}
$\mu = 2.9 \times 10^{-4}$ kg m^{-1}s^{-1}	$\mu^* = 1.3 \times 10^{-5}$ kg m^{-1} s^{-1}
$k = 6.8 \times 10^{-1}$ J m^{-1} s^{-1} K^{-1}	$k^* = 2.5 \times 10^{-2}$ J m^{-1} s^{-1} K^{-1}
$\kappa = 1.7 \times 10^{-7}$ m^2 s^{-1}	$\kappa^* = 2.0 \times 10^{-5}$ m^2 s^{-1}
$\alpha = 6.0 \times 10^{-4}$ K^{-1}	$\alpha^* = 6.0 \times 10^{-3}$ K^{-1}
$\pounds = 2.3 \times 10^6$ J kg^{-1}	$\gamma = 5.8 \times 10^{-2}$ N m^{-1}
$\gamma_T = 2 \times 10^{-4}$ Nm^{-1} K^{-1}	

TABLE 1. The physical properties used in the computations for the water–water vapour system near 100°C and 1 atm.

Having linearized the domain and boundary equations, we turn to solving for either the critical temperature drop across the bilayer system under neutral conditions or the inverse time constant, σ for a given input scaled temperature drop. In either case, the thermophysical properties and depths are held fixed.

4.2. *The linear stability calculations*

To be definite we restrict our calculations to the water–water vapour system whose properties, adopted from Huang & Joseph (1992), are given in table 1. We determine the conditions for the onset of steady motion by setting σ to zero. To justify this, a separate set of calculations was performed to obtain the values of σ when the bilayer is heated from the liquid side. It is found that the leading σ is always real regardless of the values of the input variables. Thus, neutral stability may be found by setting σ to zero. Doing this makes the scaled temperature drop across the liquid–vapour bilayer, the output 'eigenvalue'.

The eigenvalues are obtained using a Chebyshev spectral method, as outlined by Trefethen (2000). It may be observed that if the sidewalls are taken to be traction free, the variables may be separated into horizontal modes and the equations that determine the conditions for the onset of the instability are ordinary differential equations (ODEs) in the z direction. These can be easily solved by symbolic manipulation or using a numerical method. Thus, the two-dimensional code developed using the spectral method can be benchmarked against the one-dimensional solution when traction-free vertical wall conditions are employed. The agreement between the two calculations was found to be excellent, to within 1/10 %. In addition, the calculations were checked for convergence by increasing the number of spectral grid points and fourth significant place accuracy was assured for both eigenvalues and their companion eigenfunctions.

We present the results of the linearized stability calculation by making a comparison between pure evaporative instability and evaporation with the added effect of Marangoni convection. The comparison is depicted in figure 2. It shows that the addition of the Marangoni effect does not appreciably change the threshold for the onset of the instability, E_c, in the water–water vapour system. This result was also observed by Ozen & Narayanan (2004*a*), who noted that in an unbounded container, the inclusion of phase change in a bilayer heated from the liquid side actually makes the surface temperature variation weaker than it might have been in its absence. The explanation is that due to the phase change, the otherwise hot trough temperature goes down because the input energy is used to convert liquid into its vapour. An analogous argument applies to the cool crests. As a result, the phase-change action thus reduces the temperature perturbations along the interface, which in turn reduces

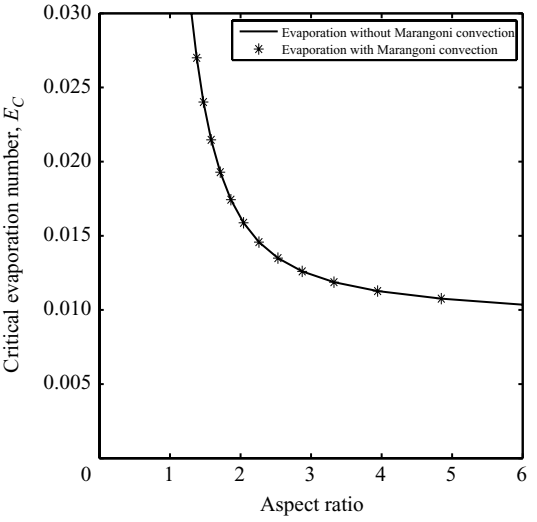

FIGURE 2. Graph of the critical evaporation number, E_c, vs. the aspect ratio, λ, showing the negligible effect of Marangoni convection in the water–water vapour system. Ra is taken to be zero. Sidewalls are assumed to be rigid, the liquid depth is 2 mm and the dimensionless vapour depth, δ, is 0.1.

surface tension gradient driven convection. Of course, this observation depends much on the magnitude of the coefficient of surface tension change with temperature. However, in the typical case of the water–water vapour system and many other systems such as alcohols and ordinary volatile organics, Marangoni convection is certainly inconsequential during evaporation into a pure vapour. This is, however, not true of Rayleigh convection where the flow does not depend upon the strength of the interfacial temperature gradients. In fact, a quick estimate of E/Ra, using the thermophysical properties given in table 1 and using reasonable liquid depths such as 1 mm, shows that the ratio is quite small and of the order of 10^{-5}. In other words, buoyancy effects cannot really be neglected even for small liquid depths unless a microgravity environment is assumed.

To understand the role of an active water vapour phase in a rigid rectangular system, we consider a concrete calculation fixing the water depth to 2 mm and only vary the depth of the vapour in two different calculations so that δ is either 0.1 or 0.2. In each case, the scaled critical temperature difference, E_c, is plotted against the aspect ratio, and in each case buoyancy convection is also assumed to take place. The results are shown in figure 3. This figure shows that increasing the depth of water vapour can make the interface more stable. This result is in agreement with the observations of Ozen & Narayanan (2004*a*) that vapour flow stabilizes the interface as the flow takes hot vapours from troughs and dumps them onto cool crests, thereby reducing the transverse temperature gradients, the interface deflections and the transverse flows. For each case, we find that increasing the aspect ratio results in the critical temperature difference approaching a constant value, thus making the bilayer system most unstable for a very large aspect ratio. This is reasonable because at large aspect ratios the thermal and momentum diffusions are small and hence the bilayer system is unstable, whereas for the small aspect ratio the thermal and momentum diffusions are large enough to dampen the disturbances of the temperature and velocity. The observation that the scaled critical temperature difference does not decrease monotonically with

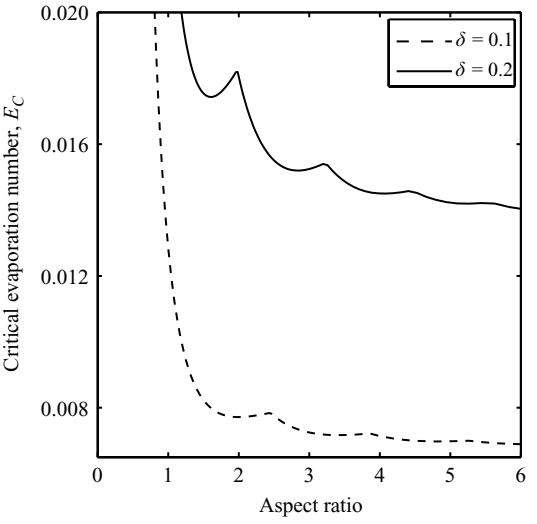

FIGURE 3. Graph of the critical evaporation number, E_c, vs. aspect ratio, λ, showing the stabilizing role of scaled water vapour depth, δ, for the case of rigid sidewalls. Rayleigh convection is assumed; the liquid depth is 2 mm.

aspect ratio is related to the inclusion of buoyancy convection in the model and is discussed below.

One might be interested in the role of rigid sidewalls on the interfacial instability. To examine this via a definite calculation, we fix the liquid depth to 2 mm while δ is again taken to be 0.1. Two computations are depicted in figure 4. In the first case, traction-free sidewalls are assumed, and in the second case rigid sidewalls are assumed. This figure shows that adding the rigid sidewall boundary condition always makes the interface more stable. This is indicated by the fact that the scaled critical temperature difference is higher than that with traction-free sidewalls. This too is reasonable since the no-slip velocity boundary condition can dampen the velocity field in the higher viscosity liquid more than the lower viscosity vapour. To assure that our reasoning is correct, we can increase the viscosity of the vapour artificially to see if the rigid sidewalls can damp out the vapour flow and thus the attendant stabilization. Indeed, we find in such calculations, not reported here, that the rigid sidewalls actually damp out the vapour flow in the case of the artificially high viscosity and thus the stability, thereby confirming that under ordinary realistic circumstances the fluid flow in the vapour is not dampened whereas the liquid flow is slowed in the presence of rigid vertical walls.

An interesting observation is that in either traction-free case or rigid sidewall case, the neutral curve is not monotonically dampened with the increase in aspect ratio. The reason is that with the change of aspect ratio, there is a competition between thermal diffusion and density gradients in the horizontal direction. And without a density gradient, Rayleigh convection cannot be generated. At very small aspect ratios, both thermal diffusion and density gradients are large. The first is stabilizing and the other promotes buoyancy flows. The stability at small aspect ratios must then be due to the strength of stabilizing thermal diffusion overwhelming the unstable density gradients. This is understandable given that thermal diffusion scales inversely with the square of the wavelength, whereas the density gradient increases inversely as the wavelength to the first power. If the aspect ratio increases, both thermal diffusion

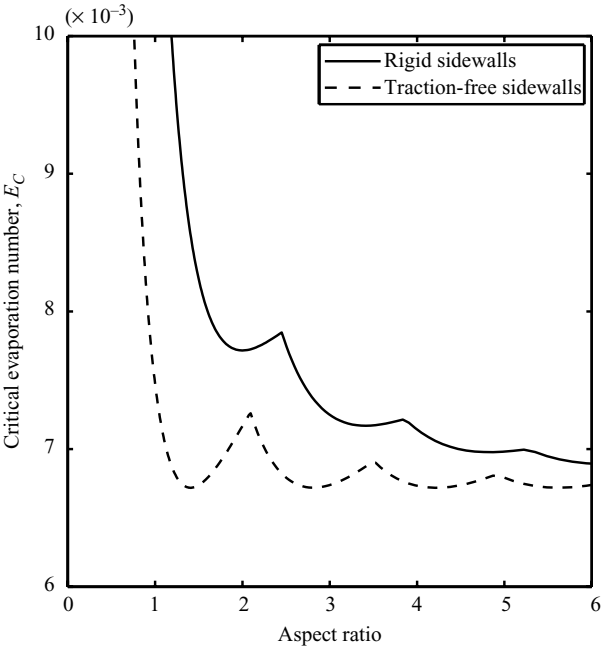

FIGURE 4. Graph of the critical evaporation number, E_c, vs. the aspect ratio, λ, showing that rigid sidewalls offer more stability than slippery walls. The liquid depth is 2 mm while the dimensionless vapour depth, δ, is 0.1. Rayleigh convection is assumed.

and density gradients are decreased. However, the thermal diffusion is clearly reduced more significantly such that the density gradients play a dominant role. As a result, the system becomes unstable.

An item of interest is the role of Rayleigh convection in the pattern formation of evaporation. To understand this, let us first turn off the effect of Rayleigh convection and give the velocity vector plot in both domains, as shown in figure 5(*a*). This figure shows that there is only one convection cell in the liquid domain indicating that multiple cellular patterns cannot be formed. However, once we turn on the effect of Rayleigh convection, we instantly find multiple convection cells, as shown in figure 5(*b*). This shows that without Rayleigh convection, multi-transverse cellular patterns cannot be formed since density gradients do not play a role; as a result, there is only one physical mechanism, viz. thermal diffusion, that can control the patterns. Once we add the second physical mechanism of density gradients, the competition kicks in and we are able to obtain multiple convection cells. The absence of multi-transverse cells in evaporative instability is not system dependent. It is a consequence of the nature of the instability. Evaporative instability is caused by the gradients in base temperature fields; here temperature perturbations at an interface are self-reinforcing, cause pressure perturbations and hence flow. Horizontal or transverse gradients of temperature are not needed to drive the instability unlike buoyancy-driven convection. Short wavelength disturbances are stabilized by diffusion and surface tension. In other words, there is no competition between mechanisms at either short or long wavelengths of disturbances. That is why pure evaporation can give rise only to single roll cells and multiple cells cannot arise. In this context it is noteworthy that evaporative instability is much like other phase-change instabilities

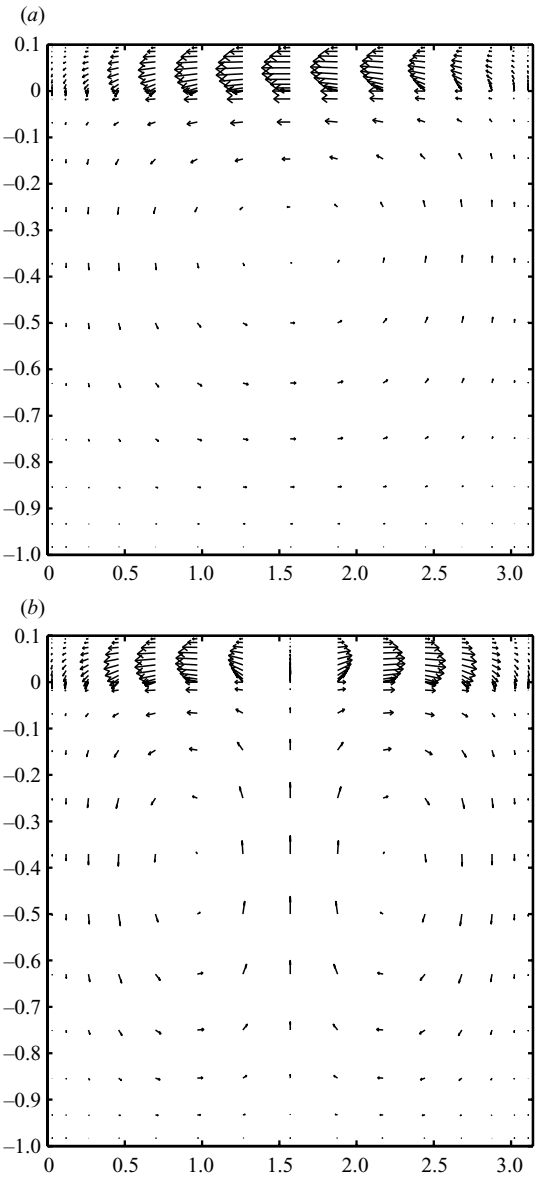

FIGURE 5. A comparison of flow profiles (*a*) without Rayleigh convection and (*b*)with Rayleigh convection showing the presence of multiple cells in the latter. The liquid depth is 2 mm, the dimensionless vapour depth is $\delta = 0.1$ and the aspect ratio is around 3. The ordinate and abscissa markings are the 'z' and 'x' positions.

such as electrodeposition, precipitation and solidification of pure materials where heat is removed from the liquid, in that the relationship of the control parameter (voltage difference in the case of electrodeposition or subcooling in solidification) versus wavenumber is monotonic. The common characteristic of these problems is that they are driven by a gradient of potential normal to the interface such as electrical or thermal and stabilized by interfacial energy and diffusion.

To summarize, the linearized stability calculations tell us that (*a*) the Marangoni effect plays a very minor role, (*b*) multi-cellular patterns are not possible with pure evaporation and that buoyancy effects must be added to create transverse cells, (*c*) flow in the vapour plays a major role in the stabilization of the interface, and (*d*) rigid sidewalls impede flow in both phases and despite the fact that vapour flows offer stability, rigid walls offer more overall stability by containing liquid phase flows compared with traction or traction-free sidewalls.

To understand what happens as we go beyond critical requires a nonlinear analysis that we now discuss.

5. Nonlinear analysis

The solution branch in the vicinity of the critical point is of interest and its nature can only be determined from a nonlinear analysis. The branching is, typically, either a pitchfork or transcritical in character. The type of bifurcation can be determined in a straightforward manner, simplified from the dominant balance method as explained by Grindrod (1991) and given in detail in the Appendix. We commence the nonlinear analysis in our problem by anticipating a forward pitchfork and look for a steady supercritical solution by increasing the scaled ΔT from its critical value by a small amount $(1/2)\epsilon^2$. If the analysis shows that the bifurcation is a backward pitchfork, then the scaled temperature drop is simply decreased from its critical value. Now the scaled temperature drop appears as Ra, Ma or E; their critical values being denoted by a subscript c. Therefore, in the case when buoyancy is included we check if a forward pitchfork obtains by advancing the scaled ΔT from its critical value, i.e. by writing

$$Ra = Ra_c + \frac{1}{2}\epsilon^2,$$

$$Ma = \frac{Ma}{Ra}\left(Ra_c + \frac{1}{2}\epsilon^2\right),$$

and

$$E = \frac{E}{Ra}\left(Ra_c + \frac{1}{2}\epsilon^2\right)$$

and observe that Ma/Ra and E/Ra are free of ΔT.

We then expand the state variables about the base state as

$$u = u_0 + \epsilon(u_1) + \frac{1}{2}\epsilon^2(u_2) + \frac{1}{6}\epsilon^3(u_3) + \cdots,$$

where the domain state variables are generically denoted by the variable 'u'.

The interface position, Z, is also expanded likewise as

$$Z = Z_0 + \epsilon Z_1 + \frac{1}{2}\epsilon^2 Z_2 + \frac{1}{6}\epsilon^3 Z_3 + \cdots.$$

Here Z_1, Z_2, etc. are the various domain mappings evaluated at the surface and must be determined in the course of our calculations at various orders.

In the case where buoyancy is ignored, we simply write

$$E = E_c + \frac{1}{2}\epsilon^2$$

whence

$$Ma = \frac{Ma}{E}\left(E_c + \frac{1}{2}\epsilon^2\right)$$

and continue as before.

We substitute the expansions of domain and surface variables into the nonlinear equations and obtain expanded equations at various orders. In considering the branching behaviour we are interested only in the steady nonlinear problem and so we set the time derivative, $\partial/\partial t$, to zero.

As in the case of the eigenvalue problem, the two-dimensional calculations were benchmarked by checking them in the case of traction-free sidewalls against the formal solution of ODEs that emanate when the variables are expanded in normal horizontal modes. The comparisons of the solutions at all orders including the value of $\boldsymbol{A}^2$ were within 0.1 %.

5.1. *Results from the nonlinear analysis*

Once we know the value of $\boldsymbol{A}$, we can calculate the actual change in the heat transfer rate or evaporation rate when we advance the control parameter beyond the critical point. The scaled heat transfer enhancement due to flow over that of conduction at the bottom plate to second order is calculated as

$$\frac{\displaystyle\int_0^{\lambda}\left(\epsilon\frac{\partial T_1}{\partial z} + \frac{1}{2}\epsilon^2\frac{\partial T_2}{\partial z}\right)\mathrm{d}x}{\displaystyle\int_0^{\lambda}\left(\frac{\mathrm{d}T_0}{\mathrm{d}z}\right)\mathrm{d}x}, \tag{5.1}$$

where $\epsilon = \sqrt{2\,|\,(E - E_c)\,|} = \sqrt{2E_c\,|\,((E/E_c) - 1)\,|}$ when pure evaporation is considered and when both buoyancy convection and evaporation are operative we have $\epsilon = \sqrt{2\,|\,(Ra - Ra_c)\,|} = \sqrt{2Ra_c\,|\,((Ra/Ra_c) - 1)\,|} = \sqrt{2Ra_c\,|\,((E/E_c) - 1)\,|}$. This last equality follows because $Ra/Ra_c = E/E_c$.

In figure 6, we have plotted the enhancement versus E/E_c for a system in which liquid depth and depth ratio are 4 mm and 0.1, respectively. The calculations are carried out assuming the physical properties of water and water vapour. Results show that when E increases over E_c by 10 %, then the heat transfer enhancement is at least as much even when Rayleigh convection is absent. Note that the heat transfer increase for traction-free sidewalls is higher than that for rigid sidewalls. This is what we expected since traction-free sidewalls have stronger flow, which can convect more heat away from the bottom plate. Taking into account the Rayleigh convection in the model, we find that the heat transfer increase is greater than the in case for which buoyancy convection is absent. This occurs even though the critical temperature drop for evaporation with buoyancy is smaller than the case of pure evaporation; it is important enough that the attendant buoyancy flow is strong and can convect substantial heat away.

Results of the weakly nonlinear analysis show that the aspect ratio and fluid depths can change the bifurcation nature. For example, in the case when the water depth is 2 mm, $\delta = 0.1$ and sidewalls are traction free, results show that the bifurcation is subcritical at large aspect ratios while supercritical bifurcation is observed at smaller aspect ratios. This is reported in table 2. However, when we keep everything else fixed and only increase the water vapour depth to $\delta = 0.2$, we find that the otherwise subcritical bifurcation turns into a supercritical one. This is also shown in table 2. In other words, the fluid depths can also change the bifurcation nature. In another

Aspect ratio	1.0	3.0	10.0
Traction-free walls ($\delta = 0.1$)	Supercritical	Supercritical	Subcritical
Traction-free walls ($\delta = 0.2$)	Supercritical	Supercritical	Supercritical
Rigid walls ($\delta = 0.1$)	Supercritical	Supercritical	Supercritical

TABLE 2. The nature of the bifurcation when the liquid depth is 2 mm, for various values of δ in the case of pure evaporation.

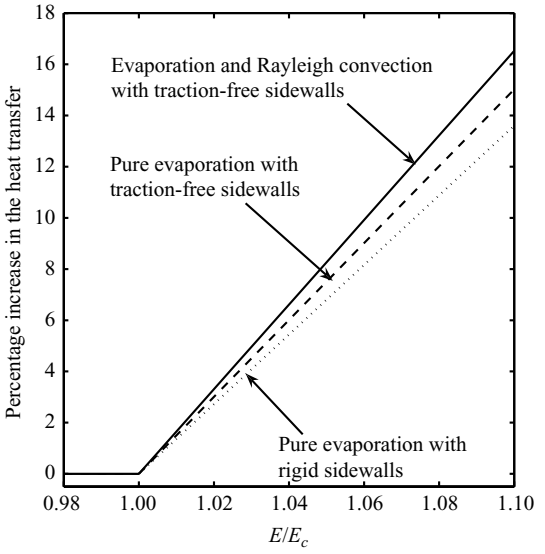

FIGURE 6. Heat transfer enhancement vs. the control parameter, E/E_c. The liquid depth is 4 mm, the dimensionless vapour depth, δ, is 0.1 and the aspect ratio is 1.

comparison, this time between the first and last rows of table 2, we can see that the boundary conditions can change the bifurcation nature unless the aspect ratio is large enough that one cannot distinguish rigid from traction-free sidewalls.

In the calculations shown in table 2, we only consider pure evaporation where Rayleigh convection is dropped. When Rayleigh convection is included, calculations done by us but not included here reveal that subcritical bifurcations turn supercritical upon increasing the liquid depth. This is due to the fact that increasing liquid depths increase buoyancy flows which in turn make the bifurcation more supercritical. This by itself comes as no surprise for it is known that pure Rayleigh convection gives only supercritical bifurcation. In addition to this observation, we find that the role of Marangoni flow is inconsequential in the post-onset regime much like its minimal role in the linearized stability problem.

6. Results of linear and nonlinear analysis for the open system

Moving to the case where we have an open container, i.e. the second case, allows the possibility that net evaporation can change in the base and perturbed states. Here, both the top and bottom walls are permeable by allowing liquid and vapour transport through a layer of porous media. In this case, the input parameters are the top pressure and the temperature difference between top and bottom walls. In

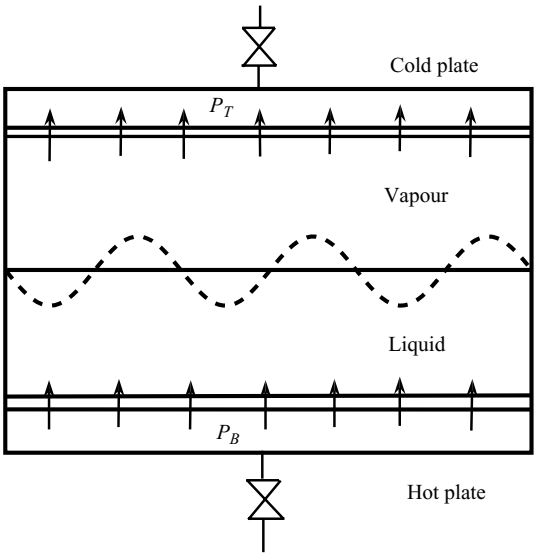

FIGURE 7. Schematic of the second case where now the valves are open and the upper and lower walls are permeable.

experiments, one can increase the temperature difference until the instability occurs, while adjusting the top pressure in such a way as to obtain a zero evaporative flux. One can then go beyond the onset condition by holding the pressure fixed thereafter and only increasing the temperature difference beyond the critical value. The second case is shown in figure 7. The unperturbed equations remain the same as before save at the top and bottom plates where they are now

$$v_z = \frac{K_{pm}}{Ld}(P_B - P) \tag{6.1}$$

and

$$v_z^* = \frac{K_{pm}}{Ld}\frac{\mu}{\mu^*}(P^* - P_T), \tag{6.2}$$

where K_{pm} is the permeability for the top and bottom media, assumed here to take realistic values, L is the media thickness, assumed here to be the same for the top and bottom walls and where d is, as always, the liquid depth. The variables P_B and P_T are the bottom and top pressures. They are assigned and are related to each other.

Let us compare the results of linear instability analysis of the first two cases in the absence of gravity. Results show that the second case is more stable in the absence of Rayleigh convection, as shown in figure 8. However, when Rayleigh convection is added, the reverse is observed, i.e. the second case is less stable in the presence of Rayleigh convection as seen in figure 9. The reason why the second case is more stable without Rayleigh convection is due to the strong vapour stabilizing flow induced by the top plate boundary condition, which is more significant than the increase in the liquid flow. However, if Rayleigh convection is added, the liquid flow gets stronger and it dominates the vapour flow making the system more unstable. It is noteworthy that unlike figure 9, figure 8 shows monotonic behaviour like the closed container case and for the same reasons. Here too, the lateral walls have only a unilateral effect on the evaporative instability unlike buoyancy-driven convection and this unilateral effect leads to monotonic behaviour.

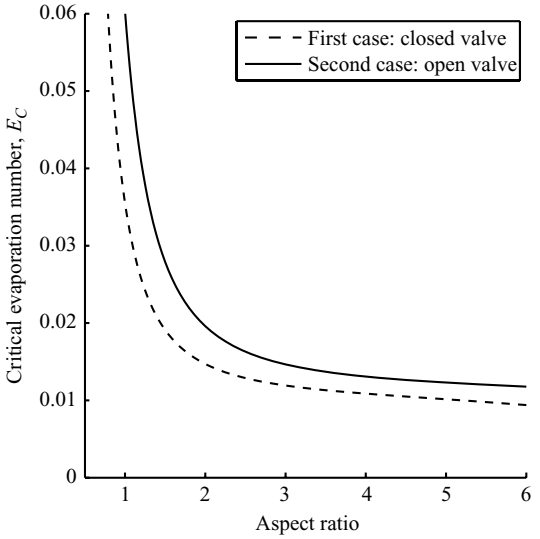

FIGURE 8. A comparison of E_c vs. aspect ratio for the two cases showing that the second case is more stable. The liquid depth is 2 mm and $\delta = 0.1$. Rayleigh convection is ignored.

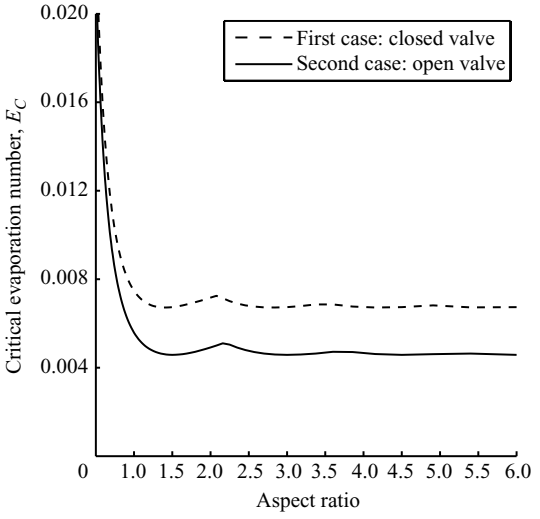

FIGURE 9. A comparison of E_c vs. aspect ratio for the two cases, Rayleigh convection taken into account showing the increased instability of the open case on account of upper and bottom porous walls. The liquid depth is 2 mm, $\delta = 0.1$.

As in the first case, the bifurcation nature, heat flux and evaporative flux are the three items of interest and arise from the nonlinear analysis. We find that for fixed fluid depths, the bifurcation nature will switch from supercritical to subcritical at large aspect ratio. This is seen in table 3, where the effect of Rayleigh convection is simply to delay the switch because of the large fluid flow. We find, as shown in figures 10 and 11, that the second case has stronger heat transfer enhancement at the bottom plate either with or without Rayleigh convection. This is reasonable given the fact that the second case has a much stronger vapour and liquid flow, which increases the heat transfer enhancement. Calculations show from the weakly nonlinear analysis

Aspect ratio	1.0	3.0	10.0	15.0
Pure evaporation	Supercritical	Supercritical	Supercritical	Subcritical
Rayleigh convection added	Supercritical	Supercritical	Supercritical	Supercritical

TABLE 3. The nature of the bifurcation when the liquid depth is 2 mm, the dimensionless vapour depth $\delta = 0.1$ with traction-free sidewalls for the open valve case.

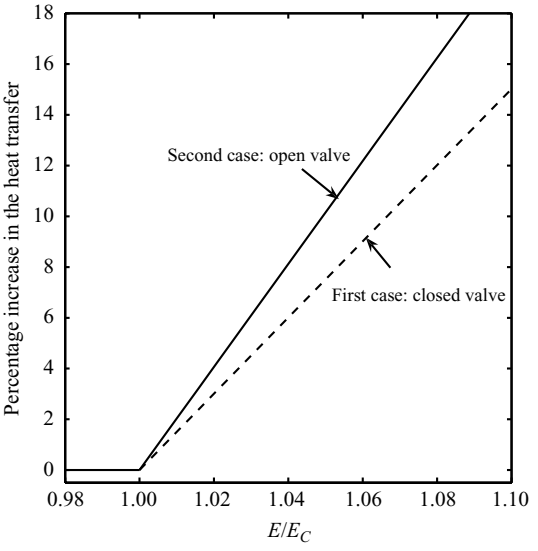

FIGURE 10. Comparison of heat transfer enhancement between the closed and open cases in the absence of Rayleigh and Marangoni convection. The liquid depth is 4 mm, the scaled vapour depth, δ, is 0.1 and the aspect ratio is 1.

that in the absence or presence of gravity there is, understandably, an increase in evaporative flux once the instability sets in. When comparing the two figures, we observe that as expected the heat transfer for the closed and open containers with Rayleigh convection lies above the corresponding curve when buoyancy convection is neglected.

7. Summary

The linear and nonlinear analyses to study the onset condition of an evaporating bilayer system in a rigid rectangular system show that (i) Marangoni convection plays a trivial role in the interfacial instability; this can be expected of all volatile systems as evaporation helps in the reduction of local hotspot temperature at the evaporating locations of an interface and, likewise, increases the local warm spots of the locally condensing parts of an interface; (ii) the vapour flow always plays a stabilizing role as it causes flow from local hot high-pressure regions towards cool low-pressure regions; (iii) rigid sidewalls always make the bilayer interface more stable because their action on suppressing liquid flow instability is more important than the suppression of vapour flow stability; (iv) open flow evaporation offers more stability than closed flow evaporation under microgravity on account of the enhanced vapour flow; this result is reversed when buoyancy convection is taken into account since

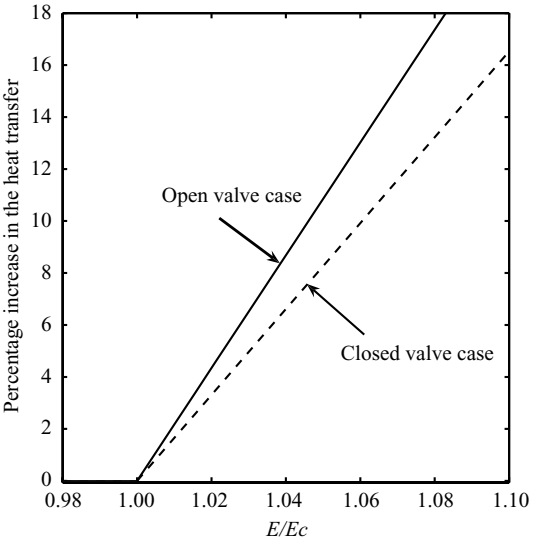

FIGURE 11. Heat transfer enhancement between both cases in the presence of Rayleigh convection, liquid depth is 4 mm, dimensionless vapour depth is $\delta = 0.1$ and aspect ratio is 1. Evaporation with Rayleigh convection.

traction or traction-free boundary conditions associated with open flow offer more buoyancy destabilization; (v) patterns generating multicellular forms are not possible in evaporation in microgravity; such patterns are associated with dominant buoyancy interference; (vi) the depth of fluids and the type of sidewall boundary conditions can change the bifurcation nature; and (vii) Rayleigh convection in the liquid side can make the bifurcation more supercritical. Although our observations are based on calculations depicted for the water–water vapour system, they have also been checked against other typical volatile systems such as ethyl alcohol. The observations and their physical explanations are therefore quite general. The calculations have shown many distinct features of evaporation but two stand out. The first is the subtle difference instability between open and closed systems. The second is the observation that like other convective flow problems, forward pitchforks (Rosenblat, Davis & Homsy 1982) are possible, and that like other phase-change problems, backward pitchforks cannot be ruled out (BuAli, Johns & Narayanan 2006).

We are grateful to the Partner University Fund and the National Science Foundation Grant CBET 0823748 for supporting travel to discuss our results with colleagues.

Appendix. The expansions of the nonlinear equations for various orders

The nonlinear analysis can be carried out by expanding the various state variables about the critical or bifurcation point.

As an example, if the bifurcation is conjectured to be a forward pitchfork, then the control parameter is advanced from its critical value by an amount $(1/2)\epsilon^2$. In other words, denoting the control variable by Λ, where Λ is simply the scaled ΔT in our problem, we write $\Lambda = \Lambda_c + (1/2)\epsilon^2$. This expansion simply defines ϵ. In response to advancing the control variables, the calculated variables, say temperature, pressure and velocity denoted by u, are assumed to take the form $u = u_0 + \epsilon u_1 + (1/2)\epsilon^2 u_2 + \cdots$. Substituting these expansions into the nonlinear equations yields equations at various

orders in ϵ whence the coefficients u_0, u_1, etc. are determined. In particular, u_1 is determined at $O(\epsilon)$ but only up to an arbitrary amplitude, $\boldsymbol{A}$, since the equation is linear and homogeneous. As the value of $\boldsymbol{A}$ is needed, we go to the second order, i.e. to the equation obtained at $O((1/2)\epsilon^2)$. The inhomogeneous terms at this order are necessarily multiples of $\boldsymbol{A}^2$ and a solvability condition is required to obtain the variables u_2.

If solvability is not satisfied then $\boldsymbol{A}^2$ must be zero and a pitchfork is not possible. This means that a transcritical bifurcation is expected and instead of our earlier assumed expansion of Λ we define ϵ via $\Lambda = \Lambda_c + \epsilon$ and proceed as before.

However, if solvability is satisfied then we must go to third order in ϵ where a balance is struck between terms that are multiples of $\boldsymbol{A}$ and those that are multiples of $\boldsymbol{A}^3$. From this balance, we get $\boldsymbol{A}^2$. If $\boldsymbol{A}^2$ is positive, we have a supercritical bifurcation and the calculation may be terminated. However, if $\boldsymbol{A}^2$ is found to be negative and equal to a value $-Q$ (for example), then the bifurcation is backward and we can see this by simply starting all over with an expansion of $\Lambda = \Lambda_c - (1/2)\epsilon^2$ only to learn that $\boldsymbol{A}^2$ is now positive and, in fact, precisely equal to Q. It is useful to note that although u_1 is an eigenfunction and is thus known up to an arbitrary constant of normalization, $\boldsymbol{A}$ is a multiple of the reciprocal of this constant and so the product $\boldsymbol{A}u_1$ is free of the constant. This simply means that it is not very useful to compare values of $\boldsymbol{A}$ for different cases. Instead, one can compare $\boldsymbol{A}u_1$ or better yet compare quantities such as the correction to heat transport at a boundary as a result of the instability.

We now proceed to give the expressions for the order expansions of the nonlinear equations for the reader who might like to try his hand at the details.

A.1. *The first-order problem*

At first order, we must determine u_1 and Z_1. The first-order problem turns out to be the same as the eigenvalue problem and we denote its solution as

$$u_1 = \boldsymbol{A}\widehat{u}_1(x, z)$$

and

$$Z_1 = \boldsymbol{A}\widehat{Z}_1(x),$$

where $\boldsymbol{A}$ is the amplitude of the solution. To investigate the nature of the bifurcation, we need to know the sign of $\boldsymbol{A}^2$. If $\boldsymbol{A}^2$ is positive, the pitchfork is forward and our expansion holds. However, if $\boldsymbol{A}^2$ is negative, the original expansion is disallowed. Instead, it must be re-expressed as $Ra = Ra_c - (1/2)\epsilon^2$, whence $\boldsymbol{A}^2$ turns out positive and the pitchfork is backward. As $\boldsymbol{A}$ cannot be determined at first order, we move onto the next order to see if we can determine the sign of $\boldsymbol{A}^2$.

A.2. *The second-order problem*

At the second order, we must determine u_2 and Z_2, and the unknown $\boldsymbol{A}$, which carries over from the first order. The domain equations at the second-order problem in the lower layer are

$$-\frac{\partial P_2}{\partial x} + \nabla^2 v_{x2} = \frac{2}{Pr}\left(v_{x1}\frac{\partial v_{x1}}{\partial x} + v_{z1}\frac{\partial v_{x1}}{\partial z}\right),$$

$$-\frac{\partial P_2}{\partial z} + \nabla^2 v_{z2} + (Ra_c T_2 + T_0) = \frac{2}{Pr}\left(v_{x1}\frac{\partial v_{z1}}{\partial x} + v_{z1}\frac{\partial v_{z1}}{\partial z}\right),$$

$$\frac{\partial v_{x2}}{\partial x} + \frac{\partial v_{z2}}{\partial z} = 0$$

and

$$\nabla^2 T_2 - v_{z2}\frac{\mathrm{d}T_0}{\mathrm{d}z} = 2\left(v_{x1}\frac{\partial T_1}{\partial x} + v_{z1}\frac{\partial T_1}{\partial z}\right).$$

Likewise, for the upper layer they are

$$-\frac{\mu}{\mu^*}\frac{\partial P_2^*}{\partial x} + \nabla^2 v_{x2}^* = \frac{\nu}{\nu^*}\frac{2}{Pr}\left(v_{x1}^*\frac{\partial v_{x1}^*}{\partial x} + v_{z1}^*\frac{\partial v_{x1}^*}{\partial z}\right),$$

$$-\frac{\mu}{\mu^*}\frac{\partial P_2^*}{\partial z} + \nabla^2 v_{z2}^* + \frac{\alpha^*}{\alpha}\frac{\nu}{\nu^*}(Ra_c T_2^* + T_0^*) = \frac{\nu}{\nu^*}\frac{2}{Pr}\left(v_{x1}^*\frac{\partial v_{z1}^*}{\partial x} + v_{z1}^*\frac{\partial v_{z1}^*}{\partial z}\right),$$

$$\frac{\partial v_{x2}^*}{\partial x} + \frac{\partial v_{z2}^*}{\partial z} = 0,$$

and

$$\nabla^2 T_2^* - \frac{\kappa}{\kappa^*}v_{z2}^*\frac{\mathrm{d}T_0^*}{\mathrm{d}z} = 2\frac{\kappa}{\kappa^*}\left(v_{x1}^*\frac{\partial T_1^*}{\partial x} + v_{z1}^*\frac{\partial T_1^*}{\partial z}\right).$$

Each of the interfacial conditions must also be expanded at second order. They are all expressed at the reference surface $z = 0$. The mass balance becomes

$$v_{z2} + 2Z_1\frac{\partial v_{z1}}{\partial z} - 2v_{x1}\frac{\partial Z_1}{\partial x} = \frac{\rho^*}{\rho}\left(v_{z2}^* + 2Z_1\frac{\partial v_{z1}^*}{\partial z} - 2v_{x1}^*\frac{\partial Z_1}{\partial x}\right). \tag{A 1}$$

At the interface, no-slip on velocity becomes

$$v_{x2} + 2Z_1\frac{\partial v_{x1}}{\partial z} + 2v_{z1}\frac{\partial Z_1}{\partial x} = v_{x2}^* + 2Z_1\frac{\partial v_{x1}^*}{\partial z} + 2v_{z1}^*\frac{\partial Z_1}{\partial x}. \tag{A 2}$$

The normal component of the force balance condition is

$$Ca\left[P_2 + 2\frac{\partial P_1}{\partial z}Z_1 - P_2^* - 2\frac{\partial P_1^*}{\partial z}Z_1 - 2\left(\frac{\partial v_{z2}}{\partial z} + 2\frac{\partial^2 v_{z1}}{\partial z^2}Z_1\right)\right.$$
$$\left. + 2\frac{\mu^*}{\mu}\left(\frac{\partial v_{z2}^*}{\partial z} + 2\frac{\partial^2 v_{z1}^*}{\partial z^2}Z_1\right)\right] + 2\frac{Ca}{Pr}v_{z1}(v_{z1} - v_{z1}^*) - BoZ_2 + \frac{\partial^2 Z_2}{\partial x^2} = 0, \tag{A 3}$$

and the tangential component of the force balance at the interface is

$$\frac{\partial v_{x2}}{\partial z} + 2Z_1\frac{\partial^2 v_{x1}}{\partial z^2} + \frac{\partial v_{z2}}{\partial x} + 2Z_1\frac{\partial^2 v_{z1}}{\partial x\partial z} + 8\frac{\partial v_{z1}}{\partial z}\frac{\partial Z_1}{\partial x}$$
$$= \frac{\mu^*}{\mu}\left[\frac{\partial v_{x2}^*}{\partial z} + 2Z_1\frac{\partial^2 v_{x1}^*}{\partial z^2} + \frac{\partial v_{z2}^*}{\partial x} + 2Z_1\frac{\partial^2 v_{z1}^*}{\partial x\partial z} + 8\frac{\partial v_{z1}^*}{\partial z}\frac{\partial Z_1}{\partial x}\right]$$
$$- \frac{Ma}{Ra}Ra_c\left[\left(\frac{\partial T_2}{\partial x} + \frac{\mathrm{d}T_0}{\mathrm{d}z}\frac{\partial Z_2}{\partial x}\right) + 2Z_1\frac{\partial^2 T_1}{\partial x\partial z} + 2\frac{\partial T_1}{\partial z}\frac{\partial Z_1}{\partial x}\right] \tag{A 4}$$

The interfacial energy balance at the second order is

$$-\left(v_{z2} + 2\frac{\partial v_{z1}}{\partial z}Z_1 - 2v_{x1}\frac{\partial Z_1}{\partial x}\right) - \frac{E}{Ra}Ra_c\left[\frac{\partial T_2}{\partial z} + 2\frac{\partial^2 T_1}{\partial z^2}Z_1 - 2\frac{\partial T_1}{\partial x}\frac{\partial Z_1}{\partial x}\right.$$
$$\left. - \frac{k^*}{k}\left(\frac{\partial T_2^*}{\partial z} + 2\frac{\partial^2 T_1^*}{\partial z^2}Z_1 - 2\frac{\partial T_1^*}{\partial x}\frac{\partial Z_1}{\partial x}\right)\right] - 4V_{PC}\frac{\partial v_{z1}}{\partial z}\left(v_{z1} - \frac{\mu^*}{\mu}v_{z1}^*\right) = 0, \tag{A 5}$$

and the continuity of interfacial temperature condition is expressed as

$$T_2 + 2Z_1\frac{\partial T_1}{\partial z} + Z_2\frac{\partial T_0}{\partial z} = T_2^* + 2Z_1\frac{\partial T_1^*}{\partial z} + Z_2\frac{\partial T_0^*}{\partial z}. \tag{A 6}$$

To close the problem at second order, we also need the interfacial phase-change boundary condition, which is

$$\Pi_{KE}\left(P_2^* + 2\frac{\partial P_1^*}{\partial z}Z_1\right) - \frac{1}{T_0^*}\left(T_2^* + 2\frac{\partial T_1^*}{\partial z}Z_1 + \frac{\mathrm{d}T_0^*}{\mathrm{d}z}Z_2\right) + \frac{1}{T^{*2}_0}\left(T_1^* + \frac{\mathrm{d}T_0^*}{\mathrm{d}z}Z_1\right)^2 - \Pi_{PE}Z_2 = 0, \quad \text{(A 7)}$$

and the constant volume condition, i.e. $\int_0^\lambda Z_2\ \mathrm{d}x = 0$. The boundary conditions at $z = \delta$ and $z = -1$ are easily expanded at second order and consequently are not given here. A comment about the constant volume requirement is in order. As mentioned earlier, the constant volume requirement is automatically met in the dynamic problem and therefore in the instability or eigenvalue problem. The steady problem, however, is different. Here constant volume simply means that the volume is held at its base value upon advancing the control variable beyond the critical. Another way of saying this is that the heights of the liquid and vapour are always held constant and kept at their base values even when the temperature difference is raised beyond its critical value.

Now the homogeneous part of the second-order problem is the eigenvalue problem. Therefore, a solvability condition must be satisfied before we can solve for u_2 and Z_2. However, the eigenvalue problem is not self-adjoint; hence, we must solve the adjoint eigenvalue problem before we can check for solvability. The adjoint eigenvectors were obtained numerically from the transpose of the matrix that results from the numerical spectral method and the bi-orthogonality requirement was checked. Even if the solvability condition is satisfied, the value of $\boldsymbol{A}^2$ cannot be determined at this order because the inhomogeneous part is a multiple of $\boldsymbol{A}^2$. We must then go to the third order with the hope of determining $\boldsymbol{A}^2$. However, if solvability is not automatically satisfied then $\boldsymbol{A}^2$ is zero, and as this is not an acceptable result we must conclude that the expansion is inappropriate and choose another expansion to advance the scaled temperature drop, i.e. $Ra = Ra_c + \epsilon$, this time expecting to see a transcritical bifurcation with subsequent determination of $\boldsymbol{A}$ at the second order. It is a simple matter to see, even without numerical computations, that for the case of slippery sidewalls, solvability is automatically satisfied. However, for the case of rigid sidewalls, this is less obvious and a numerical check on solvability is required. Computations revealed that for the case of rigid sidewalls, solvability is indeed satisfied for all values of input variables and so we proceed to third order with the expectation of determining $\boldsymbol{A}^2$.

A.3. *The third-order problem*

Similar to the second order, the third-order problem also requires that a solvability condition be satisfied in order that u_3 and Z_3 be found. This condition, then, determines the value of $\boldsymbol{A}$. To do all this requires the third-order equations. They are as follows:

For the lower layer,

$$-\frac{\partial P_3}{\partial x} + \nabla^2 v_{x3} = \frac{3}{Pr}\left(v_{x1}\frac{\partial v_{x2}}{\partial x} + v_{z1}\frac{\partial v_{x2}}{\partial z} + v_{x2}\frac{\partial v_{x1}}{\partial x} + v_{z2}\frac{\partial v_{x1}}{\partial z}\right),$$

$$-\frac{\partial P_3}{\partial z} + \nabla^2 v_{z3} + (Ra_c T_3 + 3T_1) = \frac{3}{Pr}\left(v_{x1}\frac{\partial v_{z2}}{\partial x} + v_{z1}\frac{\partial v_{z2}}{\partial z} + v_{x2}\frac{\partial v_{z1}}{\partial x} + v_{z2}\frac{\partial v_{z1}}{\partial z}\right),$$

$$\frac{\partial v_{x3}}{\partial x} + \frac{\partial v_{z3}}{\partial z} = 0$$

and

$$\nabla^2 T_3 - v_{z3}\frac{\mathrm{d}T_0}{\mathrm{d}z} = 3\left(v_{x2}\frac{\partial T_1}{\partial x} + v_{z2}\frac{\partial T_1}{\partial z} + v_{x1}\frac{\partial T_2}{\partial x} + v_{z1}\frac{\partial T_2}{\partial z}\right).$$

Likewise, for the upper layer

$$-\frac{\mu}{\mu^*}\frac{\partial P_3^*}{\partial x} + \nabla^2 v_{x3}^* = \frac{\nu}{\nu^*}\frac{3}{Pr}\left(v_{x1}^*\frac{\partial v_{x2}^*}{\partial x} + v_{z1}^*\frac{\partial v_{x2}^*}{\partial z} + v_{x2}^*\frac{\partial v_{x1}^*}{\partial x} + v_{z2}^*\frac{\partial v_{x1}^*}{\partial z}\right),$$

$$-\frac{\mu}{\mu^*}\frac{\partial P_3^*}{\partial z} + \nabla^2 v_{z3}^* + \frac{\alpha^*}{\alpha}\frac{\nu}{\nu^*}(Ra_c T_3^* + 3T_1^*) = \frac{\nu}{\nu^*}\frac{3}{Pr}\left(v_{x1}^*\frac{\partial v_{z2}^*}{\partial x} + v_{z1}^*\frac{\partial v_{z2}^*}{\partial z} + v_{x2}^*\frac{\partial v_{z1}^*}{\partial x} + v_{z2}^*\frac{\partial v_{z1}^*}{\partial z}\right),$$

$$\frac{\partial v_{x3}^*}{\partial x} + \frac{\partial v_{z3}^*}{\partial z} = 0$$

and

$$\nabla^2 T_3^* - \frac{\kappa}{\kappa^*}v_{z3}^*\frac{\mathrm{d}T_0^*}{\mathrm{d}z} = 3\frac{\kappa}{\kappa^*}\left(v_{x2}^*\frac{\partial T_1^*}{\partial x} + v_{z2}^*\frac{\partial T_1^*}{\partial z} + v_{x1}^*\frac{\partial T_2^*}{\partial x} + v_{z1}^*\frac{\partial T_2^*}{\partial z}\right).$$

For brevity, we do not provide the expansions of all boundary conditions. Only the interfacial boundary conditions are given.

The interfacial mass balance at the third order is

$$\begin{aligned} &v_{z3} + 3Z_1\frac{\partial v_{z2}}{\partial z} + 3Z_2\frac{\partial v_{z1}}{\partial z} + 3Z_1^2\frac{\partial^2 v_{z1}}{\partial z^2} - 3v_{x1}\frac{\partial Z_2}{\partial x} - \left(3v_{x2} + 6Z_1\frac{\partial v_{x1}}{\partial z}\right)\left(\frac{\partial Z_1}{\partial x}\right) \\ &= \frac{\rho^*}{\rho}\left[v_{z3}^* + 3Z_1\frac{\partial v_{z2}^*}{\partial z} + 3Z_2\frac{\partial v_{z1}^*}{\partial z} + 3Z_1^2\frac{\partial^2 v_{z1}^*}{\partial z^2} - 3v_{x1}^*\frac{\partial Z_2}{\partial x} - \left(3v_{x2}^* + 6Z_1\frac{\partial v_{x1}^*}{\partial z}\right)\left(\frac{\partial Z_1}{\partial x}\right)\right]. \end{aligned} \tag{A 8}$$

The no-slip interfacial boundary condition at the third order is

$$\begin{aligned} &3v_{z1}\frac{\partial Z_2}{\partial x} + 3\left(v_{z2} + 2Z_1\frac{\partial v_{z1}}{\partial z}\right)\left(\frac{\partial Z_1}{\partial x}\right) + v_{x3} + 3Z_1\frac{\partial v_{x2}}{\partial z} + 3Z_2\frac{\partial v_{x1}}{\partial z} + 3Z_1^2\frac{\partial^2 v_{x1}}{\partial z^2} \\ &= 3v_{z1}^*\frac{\partial Z_2}{\partial x} + 3\left(v_{z2}^* + 2Z_1\frac{\partial v_{z1}^*}{\partial z}\right)\left(\frac{\partial Z_1}{\partial x_0}\right) + v_{x3}^* + 3Z_1\frac{\partial v_{x2}^*}{\partial z} + 3Z_2\frac{\partial v_{x1}^*}{\partial z} + 3Z_1^2\frac{\partial^2 v_{x1}^*}{\partial z^2}. \end{aligned} \tag{A 9}$$

The normal stress balance at the interface is

$$\begin{aligned} Ca\Bigg\{ &P_3 + 3\frac{\partial P_2}{\partial z}Z_1 + 3\frac{\partial P_1}{\partial z}Z_2 + 3\frac{\partial^2 P_1}{\partial z^2}Z_1^2 - P_3^* - 3\frac{\partial P_2^*}{\partial z}Z_1 - 3\frac{\partial P_1^*}{\partial z}Z_2 - 3\frac{\partial^2 P_1^*}{\partial z^2}Z_1^2 \\ &- 2\left[\frac{\partial v_{z3}}{\partial z} + 3\frac{\partial^2 v_{z1}}{\partial z^2}Z_2 + 3\frac{\partial^2 v_{z2}}{\partial z^2}Z_1 + 3\frac{\partial^3 v_{z1}}{\partial z^3}z_1^2 + 12\frac{\partial v_{z1}}{\partial z}\left(\frac{\partial Z_1}{\partial x}\right)^2\right] + 2\frac{\mu^*}{\mu}\left[\frac{\partial v_{z3}^*}{\partial z}\right. \\ &\left. + 3\frac{\partial^2 v_{z1}^*}{\partial z^2}Z_2 + 3\frac{\partial^2 v_{z2}^*}{\partial z^2}Z_1 + 3\frac{\partial^3 v_{z1}^*}{\partial z^3}z_1^2 + 12\frac{\partial v_{z1}^*}{\partial z}\left(\frac{\partial Z_1}{\partial x}\right)^2\right]\Bigg\} + 3\frac{Ca}{Pr}\left(v_{z2} + 2\frac{\partial v_{z1}}{\partial z}Z_1\right. \\ &\left. - 2v_{x1}\frac{\partial Z_1}{\partial x}\right)(v_{z1} - v_{z1}^*) + 3\frac{Ca}{Pr}\left(v_{z2} + 2\frac{\partial v_{z1}}{\partial z}Z_1 - 2v_{x1}\frac{\partial Z_1}{\partial x} - v_{z2}^* - 2\frac{\partial v_{z1}^*}{\partial z}Z_1\right. \\ &\left. + 2v_{x1}^*\frac{\partial Z_1}{\partial x}\right)v_{z1} - BoZ_3 + \frac{\partial^2 Z_3}{\partial x^2} - 9\frac{\partial^2 Z_1}{\partial x^2}\left(\frac{\partial Z_1}{\partial x}\right)^2 = 0, \end{aligned} \tag{A 10}$$

and the tangential stress balance at the third order is

$$\begin{aligned}
&\frac{\mu^*}{\mu}\Bigg\{-12\left(\frac{\partial v_{x1}^*}{\partial z}+\frac{\partial v_{z1}^*}{\partial x}\right)\left(\frac{\partial Z_1}{\partial x}\right)^2+\frac{\partial v_{x3}^*}{\partial z}+3Z_1\frac{\partial^2 v_{x2}^*}{\partial z^2}+3Z_2\frac{\partial^2 v_{x1}^*}{\partial z^2}+3Z_1^2\frac{\partial^3 v_{x1}^*}{\partial z^3}\\
&\quad+\frac{\partial v_{z3}^*}{\partial x}+3Z_1\frac{\partial^2 v_{z2}^*}{\partial z\partial x}+3Z_2\frac{\partial^2 v_{z1}^*}{\partial z\partial x}+3Z_1^2\frac{\partial^3 v_{z1}^*}{\partial z^2\partial x}-6\frac{\partial v_{x1}^*}{\partial x}\frac{\partial Z_2}{\partial x}-6\left(\frac{\partial v_{x2}^*}{\partial x}+2Z_1\frac{\partial^2 v_{x1}^*}{\partial z\partial x}\right)\\
&\quad\times\left(\frac{\partial Z_1}{\partial x}\right)+6\frac{\partial v_{z1}^*}{\partial z}\frac{\partial Z_2}{\partial x}+6\left(\frac{\partial v_{z2}^*}{\partial z}+2Z_1\frac{\partial^2 v_{z1}^*}{\partial z^2}\right)\frac{\partial Z_1}{\partial x}\Bigg\}-\frac{Ma}{Ra}Ra_c\Bigg\{\left(\frac{\partial T_3}{\partial x}+\frac{\mathrm{d}T_0}{\mathrm{d}z}\frac{\partial Z_3}{\partial x}\right)\\
&\quad+3Z_1\frac{\partial^2 T_2}{\partial z\partial x}+3\frac{\partial T_1}{\partial z}\frac{\partial Z_2}{\partial x}+3Z_2\frac{\partial^2 T_1}{\partial z\partial x}+3Z_1^2\frac{\partial^3 T_1}{\partial z^2\partial x}+3\left(\frac{\partial T_2}{\partial z}+2Z_1\frac{\partial^2 T_1}{\partial z^2}\right)\left(\frac{\partial Z_1}{\partial x}\right)\Bigg\}\\
&\quad+3\frac{Ma}{Ra}Ra_c\left(\frac{\partial T_1}{\partial x}+\frac{\mathrm{d}T_0}{\mathrm{d}z}\frac{\partial Z_1}{\partial x}\right)\left(\frac{\partial Z_1}{\partial x}\right)^2-3\frac{Ma}{Ra}\left(\frac{\partial T_1}{\partial x}+\frac{\mathrm{d}T_0}{\mathrm{d}z}\frac{\partial Z_1}{\partial x}\right)\\
&\qquad=-12\left(\frac{\partial v_{x1}}{\partial z}+\frac{\partial v_{z1}}{\partial x}\right)\left(\frac{\partial Z_1}{\partial x}\right)^2+\frac{\partial v_{x3}}{\partial z}+3Z_1\frac{\partial^2 v_{x2}}{\partial z^2}+3Z_2\frac{\partial^2 v_{x1}}{\partial z^2}\\
&\qquad\quad+3Z_1^2\frac{\partial^3 v_{x1}}{\partial z^3}+\frac{\partial v_{z3}}{\partial x}+3Z_1\frac{\partial^2 v_{z2}}{\partial z\partial x}+3Z_2\frac{\partial^2 v_{z1}}{\partial z\partial x}+3Z_1^2\frac{\partial^3 v_{z1}}{\partial z^2\partial x}-6\frac{\partial v_{x1}}{\partial x}\frac{\partial Z_2}{\partial x}\\
&\qquad\quad-6\left(\frac{\partial v_{x2}}{\partial x}+2Z_1\frac{\partial^2 v_{x1}}{\partial z\partial x}\right)\left(\frac{\partial Z_1}{\partial x}\right)+6\frac{\partial v_{z1}}{\partial z}\frac{\partial Z_2}{\partial x}+6\left(\frac{\partial v_{z2}}{\partial z}+2Z_1\frac{\partial^2 v_{z1}}{\partial z^2}\right)\frac{\partial Z_1}{\partial x}.
\end{aligned}\tag{A 11}$$

The interfacial energy balance at the third order is

$$\begin{aligned}
&-3\frac{E}{Ra}\left(\frac{\partial T_1}{\partial z}-\frac{k^*}{k}\frac{\partial T_1^*}{\partial z}\right)-\left[v_{z3}+3\frac{\partial v_{z1}}{\partial z}Z_2+3\frac{\partial v_{z2}}{\partial z}Z_1+3\frac{\partial v_{z1}^2}{\partial z^2}Z_1^2-3v_{x1}\frac{\partial Z_2}{\partial x}\right.\\
&\quad\left.-3v_{x2}\frac{\partial Z_1}{\partial x}-6\frac{\partial v_{x1}}{\partial z}Z_1\frac{\partial Z_1}{\partial x}\right]+3K_{PC}v_{z1}\left(v_{z1}^2+v_{x1}^2-v_{z1}^{*2}-v_{x1}^{*2}\right)-\frac{E}{Ra}Ra_c\Bigg[\frac{\partial T_3}{\partial z}\\
&\quad+3\frac{\partial^2 T_2}{\partial z^2}Z_1+3\frac{\partial^2 T_1}{\partial z^2}Z_2+3\frac{\partial^3 T_1}{\partial z^3}Z_1^2-3\frac{\partial T_1}{\partial x}\frac{\partial Z_2}{\partial x}-3\frac{\partial T_2}{\partial x}\frac{\partial Z_1}{\partial x}-6\frac{\partial^2 T_1}{\partial z\partial x}Z_1\frac{\partial Z_1}{\partial x}\\
&\quad-\frac{k^*}{k}\left(\frac{\partial T_3^*}{\partial z}+3\frac{\partial^2 T_2^*}{\partial z^2}Z_1+3\frac{\partial^2 T_1^*}{\partial z^2}Z_2+3\frac{\partial^3 T_1^*}{\partial z^3}Z_1^2-3\frac{\partial T_1^*}{\partial x}\frac{\partial Z_2}{\partial x}-3\frac{\partial T_2^*}{\partial x}\frac{\partial Z_1}{\partial x}\right.\\
&\quad\left.-6\frac{\partial^2 T_1^*}{\partial z\partial x}Z_1\frac{\partial Z_1}{\partial x}\right)\Bigg]-V_{PC}\Bigg\{6v_{z1}\left[\frac{\partial v_{z2}}{\partial z}-2\left(\frac{\partial v_{z1}}{\partial x}+\frac{\partial v_{x1}}{\partial z}\right)\frac{\partial Z_1}{\partial x}+2\frac{\partial^2 v_{z1}}{\partial z^2}Z_1\right]\\
&\quad-12v_{x1}\frac{\partial v_{z1}}{\partial z}\frac{\partial Z_1}{\partial x}+6\frac{\partial v_{z1}}{\partial z}\left(v_{z2}+2\frac{\partial v_{z1}}{\partial z}Z_1\right)-\frac{\mu^*}{\mu}\Bigg\{6v_{z1}^*\left[\frac{\partial v_{z2}^*}{\partial z}-2\left(\frac{\partial v_{z1}^*}{\partial x}+\frac{\partial v_{x1}^*}{\partial z}\right)\right.\\
&\quad\left.\times\frac{\partial Z_1}{\partial x}+2\frac{\partial^2 v_{z1}^*}{\partial z^2}Z_1\right]-12v_{x1}^*\frac{\partial v_{z1}^*}{\partial z}\frac{\partial Z_1}{\partial x}+6\frac{\partial v_{z1}^*}{\partial z}\left(v_{z2}^*+2\frac{\partial v_{z1}^*}{\partial z}Z_1\right)\Bigg\}\Bigg\}=0,
\end{aligned}\tag{A 12}$$

and the continuity of interfacial temperature condition is

$$\begin{aligned}
T_3+3Z_1\frac{\partial T_2}{\partial z}+3Z_2\frac{\partial T_1}{\partial z}+3Z_1^2\frac{\partial^2 T_1}{\partial z^2}+Z_3\frac{\mathrm{d}T_0}{\mathrm{d}z}=T_3^*+3Z_1\frac{\partial T_2^*}{\partial z}+3Z_2\frac{\partial T_1^*}{\partial z}\\
+3Z_1^2\frac{\partial^2 T_1^*}{\partial z^2}+Z_3\frac{\mathrm{d}T_0^*}{\mathrm{d}z}.
\end{aligned}\tag{A 13}$$

To close the problem, the thermodynamic equilibrium relation between the vapour pressure and vapour temperature and the constant volume conditions is needed. The

third-order expansion of the equilibrium relation is

$$\Pi_{KE}\left(P_3^* + 3\frac{\partial P_2^*}{\partial z}Z_1 + 3\frac{\partial P_1^*}{\partial z}Z_2 + 3\frac{\partial^2 P_1^*}{\partial z^2}Z_1^2\right) - \frac{1}{T_0^*}\left(T_3^* + 3\frac{\partial T_2^*}{\partial z}Z_1 + 3\frac{\partial T_1^*}{\partial z}Z_2 + 3\frac{\partial^2 T_1^*}{\partial z^2}Z_1^2 + \frac{\mathrm{d}T_0^*}{\mathrm{d}z}Z_3\right) + 3\frac{1}{T_{base}^{*2}}\left(T_2^* + 2\frac{\partial T_1^*}{\partial z}Z_1 + \frac{\mathrm{d}T_0^*}{\mathrm{d}z}Z_2\right)\left(T_1^* + \frac{\mathrm{d}T_0^*}{\mathrm{d}z}Z_1\right) - \frac{2}{T_0^{*3}}\left(T_1^* + \frac{\mathrm{d}T_0^*}{\mathrm{d}z}Z_1\right)^3 - \Pi_{PE}Z_3 = 0. \tag{A 14}$$

At the third order, we do not have to calculate u_3 and Z_3 as our goal is to find the value of A^2. The solvability condition is sufficient to calculate its value, and once A^2 is determined the enhancement in the heat transfer can also be determined.

REFERENCES

BuAli, Q., Johns, L. E. & Narayanan, R. 2006 Geometric effects on surface roughness in electrodeposition. *IMA J. Appl. Maths* **71**, 692–714.

Burelbach, J. P., Bankoff, S. G. & Davis, S. H. 1988 Nonlinear stability of evaporating/condensing liquid films. *J. Fluid Mech.* **195**, 463–494.

Chandrasekhar, S. 1961 *Hydrodynamic and Hydromagnetic Stability*. Clarendon.

Edwards, D., Brenner, H. & Wasan, D. T. 1991 *Interfacial Transport Processes and Rheology*. Butterworth–Heineman.

Grindrod, P. 1991 *Theory and Applications of Reaction-Diffusion Equations: Patterns and Waves*. Oxford University Press.

Haut, B. & Colinet, P. 2005 Surface-tension-driven instabilities of a pure liquid layer evaporating into an inert gas. *J. Colloid Interface Sci.* **285**, 296–305.

Huang, A. & Joseph, D. D. 1992 Instability of the equilibrium of a liquid below its vapour between horizontal heated plates. *J. Fluid Mech.* **242**, 235–247.

Johns, L. E. & Narayanan, R. 2002 *Interfacial Instability*. Springer.

Margerit, J., Dondlinger, M. & Dauby, P. C. 2005 Improved 1.5-sided model for the weakly nonlinear study of Bénard–Marangoni instabilities in an evaporating liquid layer. *J. Colloid Interface Sci.* **290**, 220–230.

Margerit, J., Dondlinger, M. & Dauby, P. C. 2006 On the use of Galerkin–Eckhaus method to study the nonlinear regime of Marangoni–Bénard instabilities in an evaporating liquid layer. *Eur. Phys. J.* B **54**, 485–492.

McFadden, G. B., Coriell, S. R., Gurski, K. F. & Cotrellc, D. L. 2007 Onset of convection in two liquid layers with phase change. *Phys. Fluids* **19**, 104109.1–104109.13.

Oron, A. 1999 Nonlinear dynamics of thin evaporating liquid films subject to internal heat generation. In *Fluid Dynamics at Interfaces* (ed. W. Shyy & R. Narayanan), pp. 3–14. Cambridge University Press.

Ozen, O. & Narayanan, R. 2004*a* The physics of evaporative and convective instabilities in bilayer systems: linear theory. *Phys. Fluids* **16**, 4644–4652.

Ozen, O. & Narayanan, R. 2004*b* The physics of evaporative and convective instabilities in bilayer systems: weakly nonlinear theory. *Phys. Fluids* **16**, 4653–4660.

Ozen, O., Theisen, E., Johnson, D., Dauby, P. C. & Narayanan, R. 2005 Experiments on the role of gas height in the Rayleigh–Marangoni instability problem. *J. Colloid Interface Sci.* **289**, 271–275.

Rosenblat, S., Davis, S. H. & Homsy, G. M. 1982 Nonlinear Marangoni convection in bounded layers. Part 1. Circular cylindrical containers. *J. Fluid Mech.* **120**, 91–121.

Schrage, R. W. 1953 *A Theoretical Study of Interface Mass Transfer*. Columbia University Press.

Shankar, P. N. & Deshpande, M. D. 1990 On the temperature distribution in liquid–vapour phase change between plane liquid surfaces. *Phys. Fluids* **2**, 1030–1038.

Slattery, J. S. 1990 *Interfacial Transport Phenomena*. Springer.

Trefethen, L. N. 2000 *Spectral Methods in MATLAB*. SIAM.

Ward, C. A. & Stanga, D. 2001 Interfacial conditions during evaporation or condensation of water. *Phys. Rev.* E **64**, 051509–051517.

Zhang, N. 2006 Surface tension-driven convection flow in evaporating liquid layers. In *Surface Tension-Driven Flows and Applications* (ed. R. Savino), pp. 147–170. Research Signpost.